Applied Geochemistry 100 (2019) 213–222

Contents lists available at ScienceDirect

Applied Geochemistry

journal homepage: www.elsevier.com/locate/apgeochem

Speciation of uranium: Compilation of a thermodynamic database and its experimental evaluation using different analytical techniques

Elena L. Mühr-Ebert[a,*], Frank Wagner[b], Clemens Walther[a]

[a] Institute of Radioecology and Radiation Protection, Leibniz Universität Hannover, Herrenhäuser Straße 2, 30419, Hannover, Germany
[b] Sub-Department Groundwater Resources – Quality & Dynamics, Federal Institute for Geosciences and Natural Resources (BGR), Stilleweg 2, 30655, Hannover, Germany

A B S T R A C T

Environmental hazards are caused by uranium mining legacies and enhanced radioactivity in utilized groundwater and surface water resources. Knowledge of uranium speciation in these waters is essential for predicting radionuclide migration and for installing effective water purification technology.

The validity of the thermodynamic data for the environmental media affected by uranium mining legacies is of utmost importance. Therefore, a comprehensive and consistent database was established according to current knowledge. The uranium data included in the database is based on the NEA TDB (Guillaumont et al., 2003) and is modified or supplemented as necessary e.g. for calcium and magnesium uranyl carbonates. The specific ion interaction theory (Brönsted, 1922) is used to estimate activity constants, which is sufficient for the considered low ionic strengths. The success of this approach was evaluated by comparative experimental investigations and model calculations (PHREEQC (Parkhurst and Appelo, 1999)) for several model systems. The waters differ in pH (2.7–9.8), uranium concentration (10^{-9}-10^{-4} mol/L) and ionic strength (0.002–0.2 mol/L). We used chemical extraction experiments, ESI-Orbitrap-MS and time-resolved laser-induced fluorescence spectroscopy (TRLFS) to measure the uranium speciation. The latter method is nonintrusive and therefore does not change the chemical composition of the investigated waters. This is very important, because any change of the system under study may also change the speciation.

1. Introduction

The environmental hazard posed by geogenically increased radioactivity (NORM - Naturally Occurring Radioactive Material) in usable water resources is not limited to the remediation of contaminated sites of former uranium mining in Saxony and Thuringia or in Central Asia (Bernhard et al., 1998; Meinrath et al., 1999). Also in the exploration and utilization of new groundwater resources, for example in Burundi (Post et al., 2017), as well as in North Africa (Hakam et al., 2000, 2001a, 2001b) and the Middle East (Smith et al., 2000), NORM rather frequently poses a problem. The principle hazard associated with uranium is the potential for environmental migration through the soil, water, and air. Uranium uptake from these compartments by flora and fauna eventually leads to exposure of man. Isolation of uranium from the biosphere needs to be guaranteed on long time scales due to its long half-life ($4.5{\cdot}10^9$ years for ^{238}U). Furthermore, the radioactive daughter nuclides (of the ^{238}U decay chain), having very different environmental migration properties, need to be considered, (Skeppström and Olofsson, 2007). The chemistry of the early actinides, of which uranium is a member, can be very complicated and is mainly controlled by the pH, the redox potential, and the type of available complexing agents, such as carbonates, phosphates, and sulfates, etc. (Langmuir, 1997; Silva and Nitsche, 1995).

The redox chemistry of uranium (dominated by U(IV) and U(VI) at environmental conditions) is especially significant with respect to the mobility of uranium in the environment. The reduced species (U(lV), U^{4+}) typically precipitates from natural waters near neutral pH due to its low solubility, and so is usually characterized as relatively immobile (Silva and Nitsche, 1995). In contrast, the oxidized species of uranium, uranyl (U(VI), UO_2^{2+}), typically forms more stable aqueous complexes and is much more mobile in natural waters (Silva and Nitsche, 1995), although there are many known minerals containing uranium in the VI oxidation state (Finch and Murakami, 1999). The pentavalent uranium species (UO_2^{+}) also exists but it is less stable than the other two oxidation states and is of no relevance in the environment (Silva and Nitsche, 1995). Hydrogen ion concentration (pH) is a significant controlling factor in the speciation of uranium because solubility, sorption, complexation and colloid formation are all sensitive to solution pH (Brown and Ekberg, 2016). Natural waters vary in pH from about 2 to 10 (Silva and Nitsche, 1995), with groundwater typically ranging from 6 to 9. Equilibria are sensitive to pH, since $[H^+]$ is a component of many reactions, and therefore pH plays an important role in the determination of equilibrium component concentrations.

Predictive modelling of uranium speciation in natural waters containing NORM are often developed on the basis of thermodynamic equilibrium modelling and adequate speciation software (e.g. PHREEQC). The thermodynamic data basis readily available are partly inconsistent and not always based on the current state of knowledge.

* Corresponding author. Gesellschaft für Anlagen- und Reaktorsicherheit (GRS) gGmbH, Schwertnergasse 1, 50667 Köln, Germany.
E-mail address: elena.muehr-ebert@grs.de (E.L. Mühr-Ebert).

https://doi.org/10.1016/j.apgeochem.2018.10.006
Received 18 March 2018; Received in revised form 29 September 2018; Accepted 3 October 2018
Available online 06 October 2018

Careful attention should be payed when using such a database on the quality, up-to-datedness and range of applicability. The available thermodynamic datasets are very different in terms of completeness and consistency of uranium compounds. Furthermore, some specific databases for special applications such as in the management of radioactive waste or in geothermal systems have been developed. Generally, these are national projects selecting data restricted to use for targeted host rock, e.g. of a deep geological repository. The databases also differ in the model used to estimate activity coefficients and in the detail of the data selection documentation. The scope of ThermoChimie (Grive et al., 2015) e.g. is limited to the pH range of 6–14. Acid solutions therefore do not fall within the area of application of this database. Contrary to one's own claims, not all data are explicitly assigned references in the database and the discussion of data selection is not accessible, which makes it difficult to assess the data quality. The PSI/Nagra database (Hummel et al., 2005) was originally developed to support the performance assessment of a repository in crystalline rock, was updated to support the performance assessment of a repository in a clay formation and may not be applicable to significantly different systems. The THEREDA (Moog et al., 2015) database is based on the Pitzer approach and is limitedly operational due to the lack of interaction parameters. However, THEREDA is a work in progress and more elements, reactions and interaction parameters will be included. All of these databases are based on the NEA TDB (Guillaumont et al., 2003). The international thermodynamical database (TDB) project of the NEA (Nuclear Energy Agency), a sub-organization of the OECD, has been existing since 1986 with the aim of creating a comprehensive, internally consistent, internationally recognized and quality-assured thermodynamic database for selected chemical elements of safety relevance in the final disposal of nuclear waste. The specific ion interaction theory (SIT) was used to extrapolate experimental data to zero ionic strength. As part of the TDB project, thermodynamic data from the literature are subjected to a critical review by several international expert panels. The selected thermodynamic standard data ("selected values") and ion interaction coefficients compiled in the NEA-TDB form a consistent database (Grenthe et al., 1992; Guillaumont et al., 2003). The "Selected Values" of the NEA-TDB are an incomplete database due to the restrictive handling of the selection criteria. For practical applications, the closing of data gaps on the basis of well-founded estimates or the inclusion of less well-secured data is sometimes urgently necessary (Altmaier et al., 2011; Hummel et al., 2005; Vercouter et al., 2015).

Modelling the same water composition using different databases may lead to very different results (Mahoney, 2013) as is illustrated in Fig. 1, which compares Pourbaix diagrams of sample 2_2 with an uranium concentration of [U] = 10^{-5} mol/L (compare Table 2) calculated using a) wateq4.dat (Ball and Nordstrom, 1991) and b) the database presented in this work.

This work attempts to optimize the thermodynamic database and confirm the calculation results by measuring the speciation of uranium in the different solutions representing a broad range of natural groundwaters with high dissolved uranium using time-resolved laser-induced fluorescence spectroscopy, ion extraction on a resin, and electrospray ionization mass spectrometry.

2. Selected thermodynamic data

The quality of geochemical speciation modelling strongly depends on the applied thermodynamic database. Table 1 lists the uranium related thermodynamic data in the selected dataset including the respective reference. The data selected for the database essentially follows the NEA TDB (Guillaumont et al., 2003) recommendations and has been modified or supplemented as necessary, with the additions mainly following the recommendations of THEREDA DB (Moog et al., 2015). Major improvements of the thermodynamic data from (Guillaumont et al., 2003) regarding uranium speciation comprise several alkaline-earth-metal uranium-carbonates, some U(IV) species as well as various mineral phases. The respective ion interaction coefficients are provided in the supporting information in Table S 1 for cations and in Table S 2 for anions.

3. Experimental

The optimized thermodynamic database has been evaluated by means of model calculations and comparative laboratory tests applying time-resolved laser fluorescence spectroscopy (TRLFS), mass spectrometry and extraction experiments using different waters as model systems.

3.1. Model systems

In all experiments, synthetic waters were used to reduce the complexity of the system, for example by the presence of unknown organics. The synthetic waters were prepared by dissolving or diluting corresponding amounts of $CaCl_2{\cdot}2H_2O$ (Merck, ACS, Reag. Ph Eur), $CaCO_3$ (Merck, Reag. Ph Eur), $CaSO_4{\cdot}2H_2O$ (Fluka, p.a.), $FeSO_4{\cdot}7H_2O$ (Fluka, p.a.), H_2SO_4 (Merck, 95-95%; %, Merck, 96%, suprapur), H_3PO_4 (Fluka, 85%, ACS), HCl (VWR Chemicals, 37%), HNO_3 (VWR Chemicals, 69%, Merck, 67% suprapur), K_2SO_4 (Merck, p.a.), KCl (Merck), KOH (Merck),

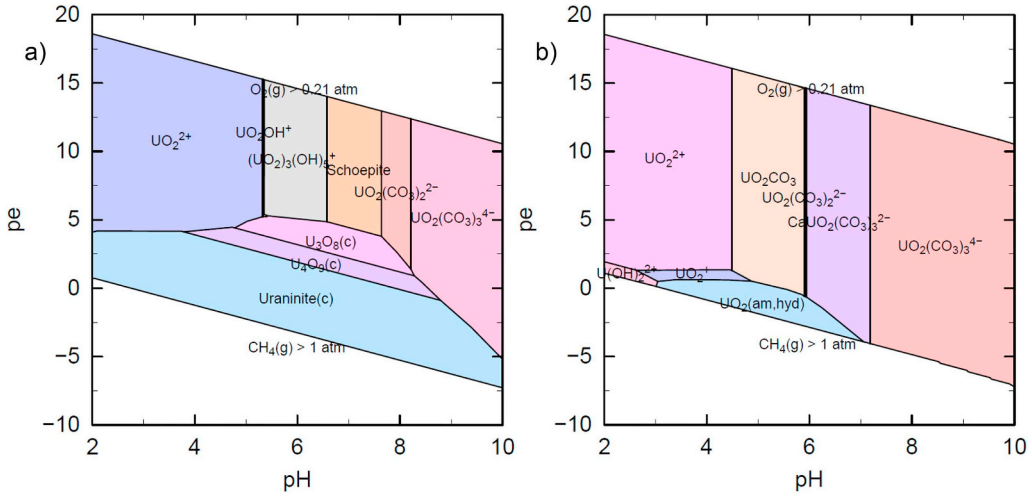

Fig. 1. Pourbaix diagrams of sample 2_2 with an uranium concentration of [U] = 10^{-5} mol/L (compare Table 2) calculated using a) wateq4.dat (Ball and Nordstrom, 1991) and b) the database presented in this work.

Table 1
Selected thermodynamic data for reactions involving uranium compounds and complexes. All data refer to the reference temperature of 298.15 K and to the standard state, i.e., a pressure of 0.1 MPa and, for aqueous species, infinite dilution (I = 0). All the values adapted from the NEA TDB (Guillaumont et al., 2003) are presented with three digits after the decimal point, regardless of the significance of these digits.

Reaction	Log K°	Ref.
Aqueous species		
$U^{4+} + e^- \rightleftharpoons U^{3+}$	−9.353	a
$4H^+ + UO_2^{2+} + 2e^- \rightleftharpoons U^{4+} + 2H_2O$	9.038	a
$UO_2^{2+} + e- \rightleftharpoons UO_2^{+}$	1.484	a
$H_2O + U^{4+} \rightleftharpoons UOH^{3+} + H^+$	−0.540	a
$H_2O + UO_2^{2+} \rightleftharpoons UO_2OH^+ + H^+$	−5.250	a
$2H_2O + UO_2^{2+} \rightleftharpoons UO_2(OH)_2 + 2H^+$	−12.150	a
$U^{4+} + 3H_2O \rightleftharpoons U(OH)_3^+ + 3H^+$	−4.7	b
$U^{4+} + 2H_2O \rightleftharpoons U(OH)_2^{2+} + 2H^+$	−1.1	b
$4OH^- + U^{4+} \rightleftharpoons U(OH)_4$	46.000	a
$3H_2O + UO_2^{2+} \rightleftharpoons UO_2(OH)_3^- + 3H^+$	−20.250	a
$4H_2O + UO_2^{2+} \rightleftharpoons UO_2(OH)_4^{2-} + 4H^+$	−32.400	a
$H_2O + 2UO_2^{2+} \rightleftharpoons (UO_2)_2OH^{3+} + H^+$	−2.700	a
$2H_2O + 2UO_2^{2+} \rightleftharpoons (UO_2)_2(OH)_2^{2+} + 2H^+$	−5.620	a
$4H_2O + 3UO_2^{2+} \rightleftharpoons (UO_2)_3(OH)_4^{2+} + 4H^+$	−11.900	a
$5H_2O + 3UO_2^{2+} \rightleftharpoons (UO_2)_3(OH)_5^+ + 5H^+$	−15.550	a
$7H_2O + 3UO_2^{2+} \rightleftharpoons (UO_2)_3(OH)_7^- + 7H$	−32.200	a
$7H_2O + 4UO_2^{2+} \rightleftharpoons (UO_2)_4(OH)_7^+ + 7H^+$	−21.900	a
$SO_3^{2-} + UO_2^{2+} \rightleftharpoons UO_2SO_3$	6.600	a
$S_2O_3^{2-} + UO_2^{2+} \rightleftharpoons UO_2S_2O_3$	2.800	a
$SO_4^{2-} + UO_2^{2+} \rightleftharpoons UO_2SO_4$	3.150	a
$U(SO_4)_2 \rightleftharpoons 2SO_4^{2-} + U^{4+}$	−10.510	a
$USO_4^{2+} \rightleftharpoons SO_4^{2-} + U^{4+}$	−6.580	a
$2SO_4^{2-} + UO_2^{2+} \rightleftharpoons UO_2(SO_4)_2^{2-}$	4.140	a
$3SO_4^{2-} + UO_2^{2+} \rightleftharpoons UO_2(SO_4)_3^{4-}$	3.020	a
$PO_4^{3-} + UO_2^{2+} \rightleftharpoons UO_2PO_4^-$	13.230	a
$HPO_4^{2-} + UO_2^{2+} \rightleftharpoons UO_2HPO_4$	7.240	a
$H_3PO_4 + UO_2^{2+} \rightleftharpoons UO_2H_2PO_4^+ + H^+$	1.120	a
$H_3PO_4 + UO_2^{2+} \rightleftharpoons UO_2H_3PO_4^{2+}$	0.760	a
$2H_3PO_4 + UO_2^{2+} \rightleftharpoons UO_2(H_2PO_4)_2 + 2H^+$	0.640	a
$2H_3PO_4 + UO_2^{2+} \rightleftharpoons UO_2(H_2PO_4)\,(H_3PO_4)^+ + H^+$	1.650	a
$CO_3^{2-} + UO_2^{2+} \rightleftharpoons UO_2CO_3$	9.940	a
$2CO_3^{2-} + UO_2^{2+} \rightleftharpoons UO_2(CO_3)_2^{2-}$	16.610	a
$3CO_3^{2-} + UO_2^{2+} \rightleftharpoons UO_2(CO_3)_3^{4-}$	21.840	a
$3\,CO_3^{2-} + UO_2^{+} \rightleftharpoons UO_2(CO_3)_3^{5-}$	6.950	a
$U(CO_3)_5^{6-} \rightleftharpoons U(CO_3)_4^{4-} + CO_3^{2-}$	1.120	a
$5CO_3^{2-} + U^{4+} \rightleftharpoons U(CO_3)_5^{6-}$	34.000	a
$U^{4+} + 2H_2O + 2CO_3^{2-} \rightleftharpoons U(OH)_2(CO_3)_2^{2-} + 2H^+$	14.36	c
$6CO_3^{2-} + 3UO_2^{2+} \rightleftharpoons (UO_2)_3(CO_3)_6^{6-}$	54.000	a
$CO_2 + 4\,H_2O + 2UO_2^{2+} \rightleftharpoons (UO_2)_2CO_3(OH)_3^- + 5H^+$	−17.358	a
$CO_2 + 4\,H_2O + 3UO_2^{2+} \rightleftharpoons (UO_2)_3O(OH)_2(HCO_3)^+ + 5H^+$	−16.028	a
$6CO_2 + 18\,H_2O + 11UO_2^{2+} \rightleftharpoons (UO_2)_{11}(CO_3)_6(OH)_{12}^{2-} + 24H^+$	−71.028	a
$UO_2^{2+} + Ca^{2+} + 3CO_3^{2-} \rightleftharpoons CaUO_2(CO_3)_3^{2-}$	27.18	d
$UO_2^{2+} + 2Ca^{2+} + 3CO_3^{2-} \rightleftharpoons Ca_2UO_2(CO_3)_3$	30.6	d
$UO_2^{2+} + Mg^{2+} + 3CO_3^{2-} \rightleftharpoons MgUO_2(CO_3)_3^{2-}$	26.13	e
Mineral phases		
$UO_2(am,hyd) = U(OH)_4(am) = UO_2{\cdot}2H_2O(am)$ $UO_2 \rightleftharpoons U^{4+} - 4OH^- - 2H_2O$	−54.500	a
Metaschoepite		
$UO_3{\cdot}2H_2O \rightleftharpoons UO_2^{2+} + 3H_2O - 2H^+$	5.350	f
Becquerelite		
$Ca(UO_2)_6O_4(OH)_6{\cdot}8H_2O \rightleftharpoons Ca^{2+} + 6UO_2^{2+} + 18\,H_2O - 14H^+$	40.500	a
Cejkaite		
$Na_4(UO_2(CO_3)_3) \rightleftharpoons 4Na^+ + UO_2(CO_3)_3^{4-}$	−5.34	A
$0.5Na_2U_2O_7 \rightleftharpoons Na^+ + UO_2^{2+} + 3OH^- - 1.5H_2O$	−29.45	a
Na-Compreignacite		
$Na_2(UO_2)_6O_4(OH)_6{\cdot}7H_2O \rightleftharpoons 17H_2O - 14H^+ + 2Na^+ + 6UO_2^{2+}$	39.400	g
Compreignacite		
$K_2(UO_2)_6O_4(OH)_6{\cdot}7H_2O \rightleftharpoons 6UO_2^{2+} + 2K^+ + 17H_2O - 14H^+$	35.800	h
$U(OH)_2SO_4 \rightleftharpoons 2OH^- + SO_4^{2-} + U^{4+}$	−31.170	a
$UO_2SO_4{\cdot}2.5H_2O \rightleftharpoons 2.5\,H_2O + SO_4^{2-} + UO_2^{2+}$	−1.589	a
$UO_2(SO_4){\cdot}3H_2O \rightleftharpoons 3H_2O + SO_4^{2-} + UO_2^{2+}$	−1.504	a
$UO_2SO_4{\cdot}3.5H_2O \rightleftharpoons 3.5H_2O + SO_4^{2-} + UO_2^{2+}$	−1.585	a
Ningoyite		
$CaU(PO_4)_2{\cdot}2H_2O \rightleftharpoons U^{4+} + Ca^{2+} + 2PO_4^{3-} + 2H_2O$	−55.920	j
Autunite		
$Ca(UO_2)_2(PO_4)_2{\cdot}3H_2O \rightleftharpoons 2PO_4^{3-} + 3\,H_2O + Ca^{+2} + 2UO_2^{2+}$	−48.360	k
Saleeite		
$Mg(UO_2)_2(PO_4)_2 \rightleftharpoons 2PO_4^{3-} + Mg^{2+} + 2UO_2^{2+}$	−46.320	l
Cernikovite (H-Autunite)		
$UO_2HPO_4{\cdot}4H_2O \rightleftharpoons 4H_2O + PO_4^{3-} + UO_2^{2+} + H^+$	−24.20	a
$UO_2(H_2PO_4)_2{\cdot}3H_2O \rightleftharpoons 2H_3PO_4^{3-} + UO_2^{2+} + 3H_2O - 2H^+$	−1.700	m
$U(HPO_4)_2{\cdot}4H_2O \rightleftharpoons 4H_2O + 2H_3PO_4 + U^{4+} - 4H^+$	−11.790	a
$(UO_2)_3(PO_4)_2{\cdot}4H_2O \rightleftharpoons 4H_2O + 2H_3PO_4 + 3UO_2^{2+} - 6H^+$	−5.960	a
$CaU_2O_7{\cdot}3H_2O \rightleftharpoons Ca^{2+} + 6H_2O - 6H^+ + 2UO_2^{2+}$	23.400	n
Rutherfordine		
$UO_2(CO_3) \rightleftharpoons CO_3^{2-} + UO_2^{2+}$	−14.760	a

a (Guillaumont et al., 2003); b (Neck et al., 2001); c (Rai et al., 1998); d (Dong and Brooks, 2006; Richter et al., 2015); e averaged value from (Geipel et al., 2008) and (Dong and Brooks, 2006); f (Altmaier et al., 2004); g (Gorman-Lewis et al., 2007) h (Gorman-Lewis et al., 2008); i (Sandino and Grambow, 1994); j (Muto et al., 1965); k (Gorman-Lewis et al., 2009), l (Muto et al., 1968); m (Schreyer and Baes, 1954); n (Altmaier et al., 2006).

Table 2
Concentrations of major ions of synthetic waters determined by ICP-OES and ion chromatography.

		1_1	1_2	2_1	2_2	3_1	3_2	4_1	4_2
pH		9.5	8.1	7.3	5.9	9.8	5.0	4.7	2.7
Na^+	mg/L	3066	1406	542	13	2320	2660	674	2110
Cl^-	mg/L	876	901	151	17	1710	1650	6.43	121
Mg^{2+}	mg/L	88	603	62	6	21	20	64	185
Ca^{2+}	mg/L	87	307	130	13	–	–	361	522
SO_4^{2-}	mg/L	3519	6632	38	14	4110	2550	1960	6190
HCO_3^-	mg/L	n.d.	n.d.	n.d.	n.d.	940	21	–	–
CO_3^{2-}	mg/L	n.d.	n.d.	n.d.	n.d.	560	–	–	–
PO_4^{3-}	mg/L	–	0.2	0.2	0.1	3.5	1000	1	1
U	mg/L	13	2	1	0.0003	9.5	–	14.2	62.6

$MgCl_2{\cdot}6H_2O$ (Merck, p.a.), $MgSO_4{\cdot}7H_2O$ (Merck; EMSURE, ACS, Reag. Ph Eur), Na_2CO_3 (Merck, ACS, ISO, Reag. Ph Eur), $Na_2CO_3{\cdot}10H_2O$ (Merck, p.a.), Na_2SO_4 (Fluka, Puriss. p.a.), $Na_3PO_4{\cdot}12H_2O$ (Merck, p.a.), and NaCl (Merck, Suprapur).

The synthetic water compositions, summarized in Table 2, represent various natural groundwaters with high dissolved uranium. The model systems have been selected to evaluate the validity of the database for uranium speciation in different hydrochemical environments. The water compositions 1 (1_1 and 1_2) and 3 (3_1 and 3_2) correspond to pore water compositions from monitoring wells in industrial tailings ponds from different uranium mining legacy sites in Saxonia/Thuringia (Eastern Germany). Since no natural water with a uranyl-phosphate dominated speciation was available, the water sample 3_2 was prepared from sample 3_1, by treating a partial solution with sodium phosphate (Na_2HPO_4 (Merck) 0.425 mol/L and NaH_2PO_4 (Merck, ASC, Reag. Ph Eur) 0.075 mol/L) to obtain a phosphate concentration of 1000 mg/L. A pH of 5.0 was adjusted by adding dilute sulfuric acid. As a consequence, uranium concentration decreased below the detection limit of the ICP-OES, which is in agreement with the modelling and discussed further in chapter 4.1. Model systems 2_1 and 2_2 correspond to groundwater samples from selected wells in Burundi in heavily weathered granite (Post et al., 2017). System 2_1, is potentially disturbed by surface water intrusion because the sampling point is located close to a lake. Two further samples correspond to groundwater samples taken from a uranium mining legacy site in Saxonia (Eastern Germany), where in-situ leaching has been applied (samples 4_1 and 4_2). In the replica of the waters only the main components, as well as the radionuclide U-238 were considered, other trace components were neglected.

The concentrations of cations in solution were measured by ICP-OES (SPECTRO ARCOS I), while concentrations of anions in solution (chloride, nitrate and sulfate) has been determined using ion chromatography (Dionex ICS 5000+) utilizing a Dionex™ IonPac™ AS19 IC

column. Phosphate concentration has been calculated based on the determination of elemental phosphor (ICP-OES). The carbonate species has been derived from sample alkalinity, which has been quantified by titration (Mettler Toledo T90) with hydrochloric acid. The pH of the samples was measured using a Orion™ Dual Star™ equipped with a Orion™ PerpHecT™ ROSS™ combination pH micro electrode both from Thermo Scientific™. Calibration was performed with technical buffer solutions pH 4.01 and 7.0 from purchased from WTW and Thermo Scientific Orion™ pH 9.18 and 12.46 buffer reference standard solution. All water samples were filtered by a 0.2 µm mixed cellulose membrane filter from Whatman prior to further treatment.

The uranium concentration in the model system 2_2 is too low for TRLFS measurements, the typical uranyl fingerprint is not visible in the spectra, strongly disturbed by scattered laser light. Therefore, a concentration series was prepared and used for further characterization of the system. The composition of the water remained unchanged except for increasing uranium concentrations of [U] = 10^{-5}, 10^{-6}, 10^{-7} and 10^{-8} mol/L.

3.2. Modelling

The measured composition of the synthesized waters (Table 2) were used as data input for the speciation modelling using PhreeqC (Parkhurst and Appelo, 1999). Because the filtered sample solutions were clear, appeared homogeneous and did not show any precipitate, undersaturation with respect to any minerals is assumed. The calculations were carried out for a temperature of 25 °C and oxygen and carbon dioxide contents in equilibrium with the atmosphere. Thus, the dissolution of oxygen and carbon dioxide is considered and the carbonate content of the solution in equilibrium is taken into account.

3.3. Time-resolved laser fluorescence spectroscopy (TRLFS)

In this work two different analysis modes of TRLFS are used. (1) Fluorescence spectra are recorded after excitation at constant laser wavelength. Band positions of the emission spectra intensity distribution depend on the chemical environments of the ions. (2) The fluorescence lifetimes of the uranyl species in solution are determined by recording the decrease in fluorescence intensity after different delay times after the (pulsed) excitation.

U(VI) luminescence spectra were measured using a Nd:YAG laser system (PS6100 series, Ekspla, Vilnius, Lithuania) operated at 50 Hz with a pulse duration of 7ns. The excitation wavelength was 266 nm with a measured laser power of 7 mW. The luminescence emission was focused into a spectrograph (Shamrock 303i, Andor Technology Ltd., Belfast, UK) with a polychromatographic grating (150 or 300 lines/mm) via fiber optics and detected using a CCD camera system (Andor iStar 743, Andor Technology Ltd., Belfast, UK). For measuring the time dependent emission decay, the delay time between laser pulse and camera gating was varied between 0 and 10000 µs. Time-resolved spectra were recorded by measuring 80–100 spectra times. For improved statistics, at each delay time, 80–100 fluorescence spectra were measured and summed.

The evaluation of the measurement data to determine the fluorescence lifetime is carried out software-based on the computer, using an in-house program. The fluorescence intensity is integrated over all uranyl bands and plotted as a function of time. The fluorescence lifetime is subsequently determined by a multi-exponential (usually mono- or bi-exponential) fit (equation (1)) to these data

$$I(t) = \sum_{i=1}^{N} A_i \cdot e^{-t/\tau_i} \quad (1)$$

Where I is the number of fitted components, A_i is a pre-exponential factor, which corresponds to the number of the emitted photons of the respective component, and τ_i is the corresponding fluorescence lifetime. The details of lifetime fitting are described, e.g., in (Kimura and Choppin, 1994) for differential lifetime measurements on uranyl in (Geipel et al., 1996) and for the method of integrated lifetime emission spectroscopy used in the present work in (Freyer et al., 2009).

Due to very strong dynamic quenching observed in measurements at room temperature, which is caused by the in some cases very high chloride contents, the measurements had to be carried out at low temperatures. Previous work has shown that under cryogenic temperatures, many of the fluorescence quenching and spectral broadening effects can be suppressed, resulting in a significant increase in spectral intensity and resolution (Wang et al., 2004, 2008). For cooling purposes, a cryostat working at liquid helium temperature (4K) is used in this work. In the present work, cooling was the only choice for obtaining spectra at all and was successfully applied to the speciation of uranyl complexes in aqueous systems (Osman et al., 2013; Steudtner et al., 2010). However, if fast kinetics are involved such as for instance hydrolysis changes in species distributions might occur.

3.4. Extraction experiments

The ratio of ternary complexes ($MUO_2(CO_3)_3^{2-}$ and $M_2UO_2(CO_3)_3$ of uranyl and carbonate with alkaline earth metals (M^{2+} corresponds to Mg^{2+} and Ca^{2+}) to anionic uranyl carbonate complexes ($(UO_2(CO_3)_x^{2(x-1)-}$) was determined by extraction experiments on an anion exchange resin. Uranium sorption on the resin corresponds to anion exchange between NO_3^- and anionic uranyl species ($(UO_2(CO_3)_3^{4-}$, $UO_2(CO_3)_2^{2-}$, $(UO_2)_2CO_3(OH)_3^-$). As described by (Dong and Brooks, 2006, 2008) the uranium absorption on the ion exchange resin in the absence of alkaline earth metals in the pH range of 7–10 leads to a constant distribution coefficient D (equation (2)) of 25760 mg/L.

$$D = \frac{[U(VI)]_R}{[U(VI)]_{aq}} \quad (2)$$

M-UO_2—CO_3-complexes are not or only weakly adsorbed on the anion exchange resin (Dong and Brooks, 2006), allowing one to calculate the proportion of these complexes in the solution from the determined partition coefficient. Extraction experiments were carried out for the model systems 1_1, 1_2, 2_1, and 3_1. For the remaining model systems, corresponding investigations were not useful, because at the corresponding pH no anionic uranyl species are expected for sample 2_2, the uranium concentration in sample 3_2 was below the detection limit of the ICP-OES and samples 4_1 and 4_2 do not contain any carbonate. Gel Type Amberlite IRA-410 strong base anion exchange resin was purchased from Sigma-Aldrich (St. Louis, MO) in the chloride form and converted to the nitrate form prior to use as described in (Dong and Brooks, 2006). Uranium batch adsorption experiments were carried out at 25 °C and atmospheric CO_2 in 50 ml polyethylene bottles using 20 ml solution and 0.05 g air-dry resin. The suspensions were equilibrated on a shaker for 5 days. Thereafter, the solution was filtered and prepared by acidification for U(VI) and metal quantification. The resin beads were separated by filtration, rinsed rapidly with three 5 ml aliquots of distilled water, and transferred to 2.5 ml of 1% HNO_3 in a 10 ml polyethylene bottle. Desorbed metals were quantified after an extraction period of three days either by ICP-MS or ICP-OES.

Aqueous Mg, Ca and U concentrations were measured using inductively coupled plasma mass spectrometry (ICP-MS, iCAP Q from ThermoFisher), autosampler Cetac ASX-520, concentric atomizer, quartz cyclone spray chamber with inner tube, plasma power 1550 W) and inductively coupled plasma optical emission spectrometry (ICP-OES) with an iCAP 6200 Duo from ThermoFisher (iTeva Software, Cetac ASX-260 autosampler, Mira-Mist nebulizer, cyclone spray chamber, 1150 W plasma power) or an ARCOS from Spectro Analytical Instruments GmbH (Kleve, Germany).

The measured amount of desorbed metal was used to determine the

corrected U(VI) distribution coefficients, as described in (Dong and Brooks, 2006). This takes into account the possibility that $MUO_2(CO_3)_3^{2-}$ and $M_2UO_2(CO_3)$ could be adsorbed to the resin according to the following exchange reactions

$$2RNO_3^- + MUO_2(CO_3)_3^{2-} \rightleftharpoons (R^+)_2MUO_2(CO_3)_3^{2-} + 2NO_3^- \quad (3)$$

$$2RNO_3^- + M_2UO_2(CO_3)_3^0 \rightleftharpoons (R^+)_2MUO_2(CO_3)_3^{2-} + 2NO_3^- + M^{2+} \quad (4)$$

Where R^+ is the functional group of the anion-exchange resin.

To address this issue (Dong and Brooks, 2006), developed a correction procedure. The total amount of M^{2+} on the resin phase, either $(R^+)_2MUO_2(CO_3)_3^{2-}$ associated or entrained in the resin pore water, was extracted and quantified in acidic solution (1% HNO_3) by the aforementioned desorption process. The amount of M^{2+}, corresponding to $(R^+)_2MUO_2(CO_3)_3^{2-}$, M_R (µmol), was obtained from equation (5)

$$M_R = C_d \cdot V_d - C_b \cdot \frac{m_W \varepsilon}{\rho_W} \quad (5)$$

With the total metal concentration in the desorption solution C_d (µmol/mL), the volume of desorption solution V_d (mL), the metal concentration in the equilibrated bulk solution C_b (µmol/mL) (here M^{2+} concentration in resin pore water is assumed to equal that in the bulk solution at equilibrium), the solution density ρ_W (g/cm^3), the mass (g) of wet resin m_W, and the fractional water content of wet resin ε. According to the stoichiometric ratio, M_R (µmol) should correspond to the amount of U(VI) associated with $(R^+)_2MUO_2(CO_3)_3^{2-}$. Thus, M_R was used to correct the distribution coefficient D (equation (2)) by subtracting M_R/m from the total absorbed $[U(VI)]_R$ and adding M_R/V to the aqueous phase $[U(VI)]_{aq}$.

3.5. Orbitrap mass spectrometry

The mass spectrometric measurements were carried out on a hybrid mass spectrometer Orbitrap Elite (Thermo Fisher Scientific, Waltham, Massachusetts, USA) equipped with a Nanospray Flex Ion Source. Nano-ESI needles were purchased from New Objective Inc (Woburn, MA, USA). The evaluation of the obtained spectra was carried out with the Xcalibur software (Thermo Fisher Scientific, Waltham, Massachusetts, USA). For each sample, a mass spectrum was recorded for 30 s and the intensities were then averaged over time.

4. Results and discussion

4.1. Modelling

Species distributions for the model systems are calculated by PhreeqC using the database equilibrium constants of Table 1. All uranium species with a relative abundance exceeding 0.01% are plotted in Fig. 2. The polymeric species are weighted with respect to their number of uranyl units.

The results for the model system 1_1 and 1_2 are very similar and dominated by alkaline-earth-metal uranium-carbonates. The same applies for sample 2_1, while 2_2 is dominated by UO_2CO_3. This system is characterized by a lower pH and a significantly lower concentration of uranium. Since the concentrations of calcium and magnesium are low, sample 3_1 is dominated by uranyl carbonate. Samples 4_1 and 4_2 are acidic waters with high sulfate content and are therefore dominated by uranyl sulfates.

Sample 3_2 was prepared from sample 3_1 by addition of phosphate ions. Uranium speciation is not shown in Fig. 1, since speciation modelling revealed the appearance of some supersaturated uranyl phosphate phases of low solubility, namely uranyl phosphate, autunite, and saleeite. A precipitate was not observed visually, due to the low U(VI) concentration and the resulting small amount of precipitate. The TRLFS measurement delivered no signal, regardless of the delay time, which also indicates precipitation of the U(VI) most likely phosphate compounds. The uranium concentration in sample 3_2 was below the detection limit of the ICP-OES. The modeled species distribution based on sample 3_1, and the addition of phosphate and pH change, taking the precipitation of supersaturated phases into account, predicted $4{\cdot}10^{-6}$ mol/L of dissolved uranium, which is one order of magnitude less compared to sample 3_1.

The results for the dilution series of sample 2_2 are shown in Fig. 3 together with those for the actual system. The uranium speciation in the systems are relatively similar for uranium concentrations between 10^{-9} and 10^{-7} mol/L and change dramatically as the concentration is further increased. At a uranium concentration of 10^{-5} mol/L, uranylhydroxocarbonate is the dominant uranium species.

4.2. Cryogenic time resolved laser fluorescence spectroscopy

To evaluate the thermodynamic calculations, all water samples were measured by TRLFS. Uranium speciation can be obtained from the characteristic lifetimes and the fluorescence wavelengths of the different complexes. Fig. 4 displays the TRLFS spectra of sample 1_1 measured at low temperature (4 K)with delay times between 0.1 and 5 ms. A detailed comparison of the emission band positions of the model systems together with reference data from (Wang et al., 2004) is given in Table 3.

Calcium uranyl carbonate can be assigned as the dominant species for samples 1_1, 1_2, and 2_1, which is in agreement with the calculations. However, the two calcium uranyl carbonates ($CaUO_2(CO_3)_3^{2-}$ and $Ca_2UO_2(CO_3)_3$) cannot be distinguished by TRLFS. Additionally, fluorescence lifetimes were determined for the model systems as described above. They are also included in Table 3. For the samples 1_1, 1_2, and 2_1, the longer lifetime can be attributed to the calcium uranyl carbonate, which has already been identified as the dominant species by the band position. A second species cannot be unambiguously assigned.

A comparison of the emission maxima of sample 3_1 with literature data (Table 3) identifies $UO_2(CO_3)_3^{4-}$ as the most abundant uranium (VI)species. This finding corroborates the results of the speciation calculation. The calculated fluorescence lifetimes for sample 3_1 cannot be clearly assigned to any species. The longer calculated lifetime of 1045 µs agrees reasonably well with the literature value of the uranium (VI) species of the highest expected abundance $UO_2(CO_3)_3^{4-}$, whose lifetime may be overestimated as the lifetimes of $UO_2(CO_3)_3^{4-}$ (τ = 883 µs) and $CaUO_2(CO_3)_3^{2-}$ (τ = 1282 µs) cannot be resolved. The shorter lifetime (τ = 241 µs) most closely matches the one of $MgUO_2(CO_3)_3^{2-}$, although the lifetime is greater than expected. The reason might originate from the process of data fitting: A biexponential function is characterized by five parameters that are to some extent covariant limiting the robustness of each individual parameter of the fit.

The emission maxima of sample 4_1 are compared in Table 3 with literature data by (Wang et al., 2004) for different uranyl species. The emission band positions most closely match the calcium uranyl carbonate complex, but this is not consistent with its very long lifetime of 1282 µs. A comparison with the water analysis (Table 2) also excludes a calcium uranyl carbonate complex, since the water contains no carbonate. Unfortunately, for uranyl sulfate complexes, no comparative data is available at low temperatures. The time resolved spectroscopy of sample 4_1 gave two lifetimes. The shorter one matches the lifetime of the free uranyl cation of τ = 270 µs (Wang et al., 2004) at 4 K. While this assignment is rather plausible, spectral band positions do not match. The longer life time of τ = 747 µs cannot be assigned to any species expected based on the modelling. The band positions and fluorescence lifetime determined for sample 4_2 correspond most likely to the free uranyl ion.

According to the thermodynamic modelling (compare Fig. 2),

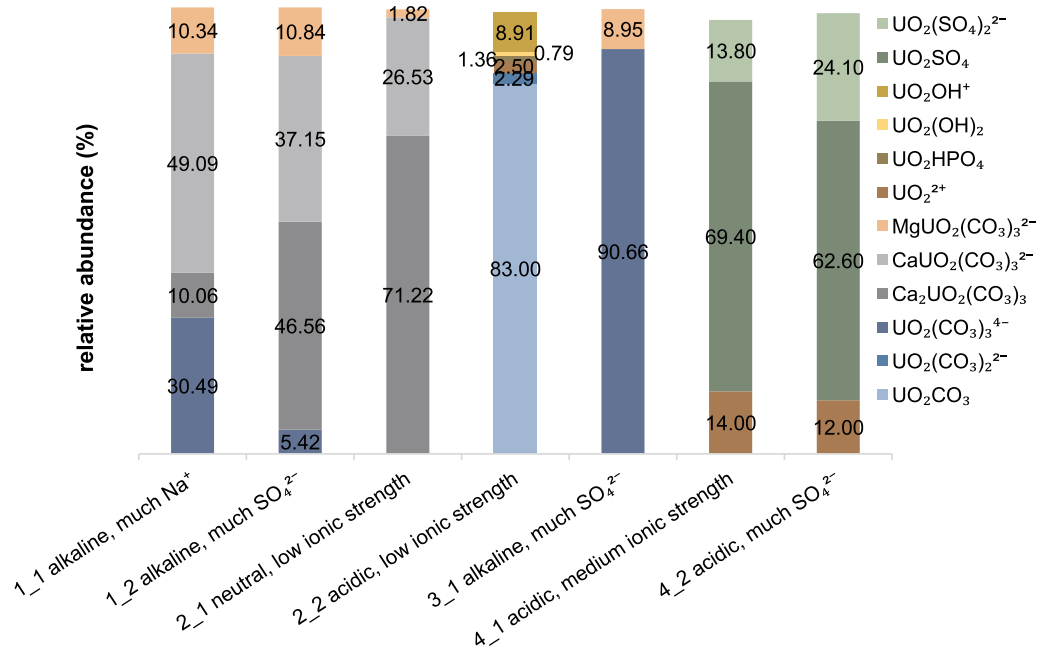

Fig. 2. Calculations of the speciation of the model systems applying PhreeqC based on the created database. All uranium species with a relative abundance of more than 0.1% are plotted. The polymeric species are weighted with respect to their number of uranyl units.

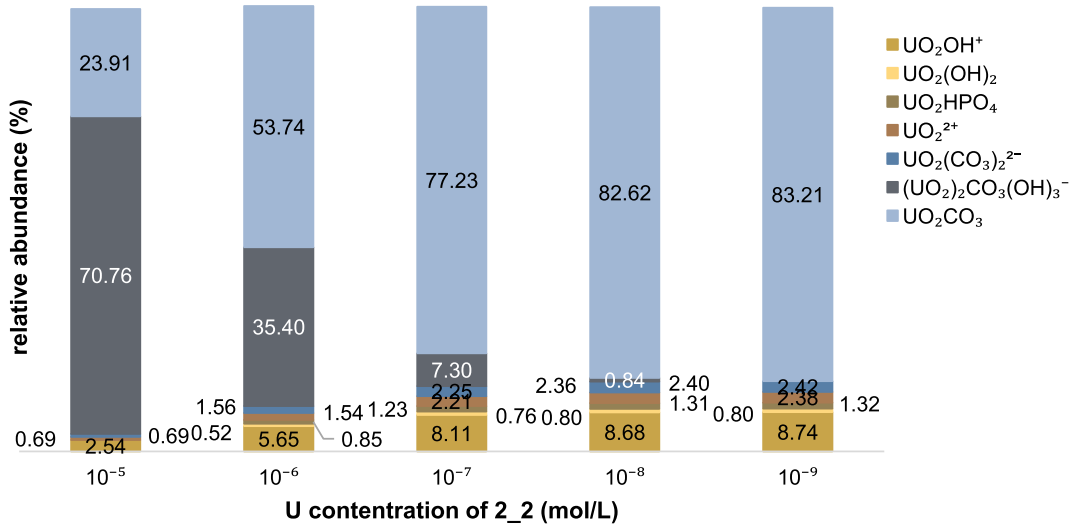

Fig. 3. Calculations of the speciation of the model system 2_2 with different uranium concentrations in mol/L using PhreeqC and equilibrium constants of the created database. All uranium species with a relative abundance of more than 0.1% are plotted. The polymeric species are weighted with respect to their number of uranyl units.

uranyl sulfate is expected to be the principal (most abundant) species in sample 4_2. As with sample 4_1, however, a comparison with the literature for the sulfate species is not possible. The free uranyl ion, which in band position and lifetime agrees well with the literature, has an expected relative abundance of 12.0% in this sample.

The band positions of the samples from the dilution series of system 2_2 with uranium concentrations of 10^{-5}, 10^{-6}, and 10^{-7} mol/L agree quite well. The matching bands are slightly shifted to shorter wavelengths compared to the $UO_2CO_{3(aq)}$. The time resolved spectroscopy results in lifetimes around 600 µs for all three samples which can be assigned to $UO_2CO_{3(aq)}$. For samples with higher uranium concentrations (10^{-5} and 10^{-6} mol/L) a second shorter lived species was detected and can be assigned as $(UO_2)_2CO_3(OH)_{3-}$, which is in good agreement with the modelling results. Table 4 summarizes the results of the cryo-TRLFS investigations.

4.3. Time resolved laser fluorescence spectroscopy at room temperature

Due to the lack of reference data for TRLFS measurements of uranyl sulfate at low temperature, additional investigations were performed for samples 4_1 and 4_2 at room temperature. Due to quenching effects, the signal to noise ratio was rather low as can be seen in Fig. 5 and the evaluation of the lifetimes was difficult. Nevertheless, two fluorescence lifetimes were determined for both samples.

In the case of sample 4_2 the shorter fluorescence lifetime agrees very well with $UO_2(SO_4)_2^{2-}$ (compare Table 5), while the positions of the emission bands are slightly shifted to higher wavelengths. While $UO_2(SO_4)_2^{2-}$ is identified as major species on the basis of the measurement, UO_2SO_4(aq) is expected as most abundant species in this sample as can be seen in Fig. 2. However, distinguishing the uranyl sulfate complexes based on the band position is difficult because the

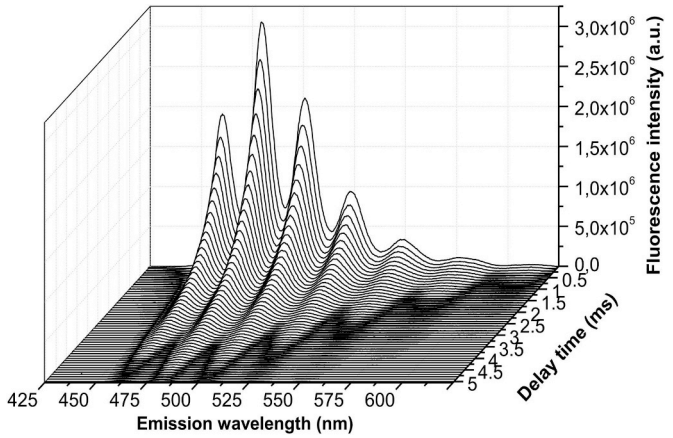

Fig. 4. Set of time-resolved fluorescence spectra with delay times between 0.1 and 5 ms for sample 1_1 at low temperature (4 K).

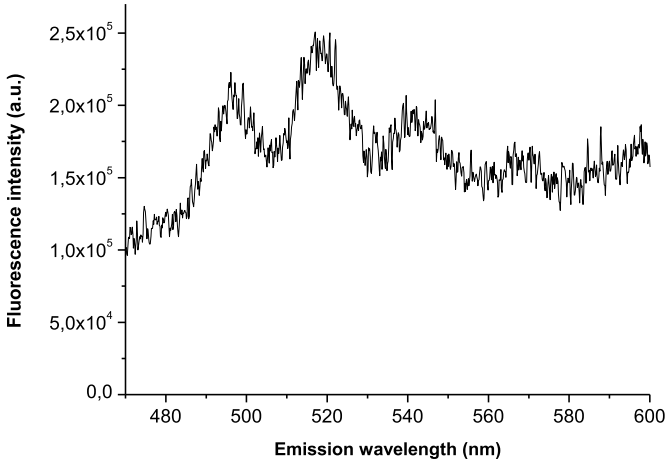

Fig. 5. Fluorescence spectrum with a delay time of 1 µs for sample 4_2 at room temperature.

Table 3
A comparison of TRLFS measurements of the model systems with spectroscopic data for model complexes (Wang et al., 2004) and own spectroscopic data for $MgUO_2(CO_3)_3^{2-}$ (details are provided in the Supporting Information). All measurements were conducted at liquid helium temperature.

Species/sample	Main emission wavelengths (nm)	τ (µs)
UO_2^{2+}	492–514 – 538–564 – 592	270
$(UO_2)_2CO_3(OH)_3^-$	523–542 – 561	144
UO_2CO_3	479–498 – 519–542 – 567	465
$UO_2(CO_3)_2^{2-}$	477–496 – 517–540 – 564	962
$UO_2(CO_3)_3^{4-}$	480–499 – 520–542 – 566	883
$Ca_xUO_2(CO_3)_3^{2(2-X)-}$	481–501 – 523–546 – 572	1282
$MgUO_2(CO_3)_3^{2-}$	479–498 – 519–541	170
1_1	481–501 – 524–549 – 578	512 ± 44; 1237 ± 62
1_2	482–503 – 526–552 – 579	606 ± 128; 1404 ± 69
2_1	480–502 – 524–549 – 574	479 ± 27; 1155 ± 13
2_2 (U 10^{-5} mol/L)	475–494 – 514–536	118 ± 32; 604 ± 100
2_2 (U 10^{-6} mol/L)	470–493 – 514–530	129 ± 28; 666 ± 26
2_2 (U 10^{-7} mol/L)	475–494 – 514–536	519 ± 281
3_1	480–499 – 520–541 – 565	241 ± 15; 1045 ± 9
3_2	–	–
4_1	481–501 – 522–544	230 ± 5; 747 ± 12
4_2	490–512 – 535–558	240 ± 90

positions of the main emission bands are very similar (Vercouter et al., 2008). The longer fluorescence lifetimes cannot be assigned to any species expected on the basis of the modelling results. For sample 4_1 an assignment is not possible on the basis of the TRLFS investigation at room temperature. The difficulties in the interpretation are caused by the rather low quality of the TRLFS measurements at room temperature, which is due to quenching effects as discussed above, and do not necessarily point to an inaccuracy in the thermodynamic data.

Table 5
A comparison of TRLFS measurements of the model systems with spectroscopic data for model complexes from (Bernhard et al., 1996). All measurements were conducted at room temperature.

Species/sample	Main emission wavelengths (nm)	Lifetime τ (µs)
UO_2^{2+}	488–510 – 532–558	2.70 ± 0.5
UO_2SO_4(aq)	493–514 – 538–565	4.3 ± 1.0
$UO_2(SO_4)_2^{2-}$	493–514 – 538–565	11.0 ± 2.0
$UO_2(SO_4)_3^{4-}$	493–514 – 538–565	18.3 ± 3.0
4_1	486–505 – 526	7.7 ± 1.2; 150 ± 1.3
4_2	498–519 – 540–565	12.3 ± 3.4; 306 ± 42.2

4.4. Extraction experiments

From the uranium concentrations in the elution and desorption solutions, respectively, distribution coefficients D_M are calculated and corrected according to Dong et al.(Dong and Brooks, 2006) They are given in Table 6 along with relative abundances of $UO_2(CO_3)_x^{2(x-1)-}$ and $M_xUO_2(CO_3)^{2(2-x)-}$ and calculated values. The proportion of anionic uranyl carbonates determined in the extraction experiments for the model systems 1_1, 1_2, and 3_1 is significantly lower than what is expected from the model calculations. The distribution coefficient for $UO_2(CO_3)_3^{4-}$ D_0 is 25760 ml/g for the resin Amberlite IRA-410 according to (Dong and Brooks, 2006). For sample 3_1, the distribution coefficient D_M is 15363 mL/g, which corresponds to a proportion of $UO_2(CO_3)_3^{4-}$ of 59.6%. The modelling gives an expected abundance of 90.7% (see Fig. 2). However, the experimental result and the calculation agree within the order of magnitude. Uncertainties in the extraction experiments lie in the quantitative transfer of the resin, the simplification that the only absorbed species was $UO_2(CO_3)_3^{4-}$ and measurement uncertainties in the analysis. The overall trend is in line

Table 4
Summary of the cryo-TRLFS investigation. All identified species are denoted with X.

	1_1	1_2	2_1	2_2 (10^{-5})	2_2 (10^{-6})	2_2 (10^{-7})	3_1	4_1	4_2
UO_2^{2+}								X	X
$(UO_2)_2CO_3(OH)_3^-$				X	X				
UO_2CO_3				X	X	X			
$UO_2(CO_3)_3^{4-}$							X		
$Ca_xUO_2(CO_3)_3^{2(2-X)-}$	X	X	X						
$MgUO_2(CO_3)_3^{2-}$							X		

Table 6
Results of the extraction experiments on the carbonate containing model systems with gel-type Amberlite IRA-410 strongly basic anion exchange resin compared to the modelling results.

	D_M	$UO_2(CO_3)_x^{2(x-1)-}$ (%)	$M_xUO_2(CO_3)^{2(2-x)-}$ (%)	Calc. $UO_2(CO_3)_x^{2(x-1)-}$ (%)
1_1	2681	10.4	89.6	30.5
1_2	220	0.9	99.1	5.4
2_1	494	1.9	98.1	0.4
3_1	15364	59.6	40.4	90.7

with expectations.

Between 0.007 and 0.024 µmol magnesium and up to 0.05 µmol calcium metal adsorb on the anion exchange resin in the extraction experiments. Adsorbed magnesium and calcium were found in all samples, except for calcium in sample 3_1 (Dong and Brooks, 2006). reported no metal adsorption to the resin in uranium-free controls. Accordingly, the metals adsorbed in the present study can be assigned to the alkaline-earth-metal uranium-carbonates, and thus a qualitative detection of these species has taken place.

4.5. Orbitrap mass spectrometry

The samples from the dilution series of the model system 2_2 with uranium concentrations of 10^{-5}-10^{-7} mol/L were further analyzed by an electrospray Orbitrap mass spectrometer. The source was operated in positive mode because the uranyl hydroxide (UO_2OH^+) cation was expected to be the second most abundant species besides the uncharged uranyl carbonate (UO_2CO_3). In order to simplify spectra evaluation, high-purity chemicals were used. Nevertheless, the spectra are dominated by the background electrolyte. Only a few additional peaks in the solutions could be identified and attributed to uranium species.

The peaks at mass to charge ratios of 323.06 and 305.05 and 287.04 can be assigned to the uranyl hydroxide ion carrying different numbers of water molecules in the solvent shell. The water molecules are a remnant of the ESI process, where the evaporation of the solvent was not complete. While this effect increases the number of peaks it is nevertheless desirable because it demonstrates soft ionization by the ESI process. Furthermore, additional peaks in the spectra can be assigned to the uranyl ion (UO_2^{2+}) carrying one or two water molecules. The uranyl ion (UO_2^{2+}) appears as a singly-charged species, but it is known from previous ESI-MS studies that uranyl undergoes partial reduction after desolvation, resulting in a UO_2^+ peak at 270.04 m/z and 288.05 and 306.06 respectively (Agnes and Horlick, 1992; Galindo and Del Nero, 2013; Moulin et al., 2000). Uranyl hydroxide, as just described, could be identified as the dominant positively charged species in all samples of the dilution series. Fig. 6 compares the intensities of the peaks of uranyl hydroxide with 0, 1 and 2 water molecules and free uranyl with one or two water molecules. The intensity of the peaks increases with increasing uranium concentration and the number of water molecules. As can be seen from the diagram, the intensity of the peaks increases with the uranium concentration and the number of water molecules, with no more than two water molecules in the solvation shell. The stability of the measurements and the associated reproducibility do not allow absolute quantification, but only a comparison of the intensities with each other.

4.6. Comparison of modelling and experimental results

The results of the model calculations are summarized in Table 7, the calculated relative abundances are given as percentage and are printed in bold for all species confirmed experimentally. In addition, for all species with expected relative abundances greater than one percent, which could not be confirmed experimentally, the absolute concentrations in mol/L are given in parentheses. For species with relative abundances < 0.1% or equal to zero the value is omitted for the sake of clarity.

For all investigated neutral and alkaline systems, at least the two, in most cases the three, species with the highest expected relative abundances could be confirmed. All species with expected concentrations > 10^{-7} mol/L were detected. It should be noted that $Ca_2UO_2(CO_3)_3$ and $CaUO_2(CO_3)_3^{2-}$ cannot be distinguished by the chosen methods. The same applies to the detection of $UO_2(CO_3)_3^{4-}$ and $UO_2(CO_3)_2^{2-}$ in the extraction experiments. Low temperature spectroscopic data of $MgUO_2(CO_3)_3^{2-}$ has been obtainied for the first time using TRLFS (Supplementary Information).

For the acidic waters of the mining area Königstein, however, there are contradictions to the model calculations. Based on the model calculation, $UO_2SO_{4(aq)}$ is the dominating uranium species for both waters, while the emission bands of the two solutions are clearly shifted from each other both at low and room temperature. On the other hand, the

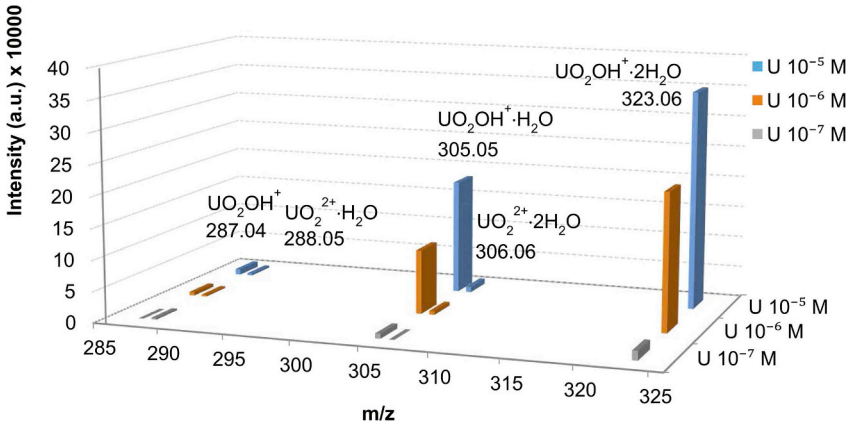

Fig. 6. Comparison of the peak intensities of uranyl hydroxide with zero, one or two water molecules and free uranyl with one or two water molecules in mass spectra of model system 2_2 with different uranium concentrations.

Table 7
Summary of the results of the model calculations, the calculated relative abundances are given as a percentage. The polymeric species are weighted with respect to their number of uranyl units. For species with relative abundances < 0.1% or equal to zero the value is omitted for the sake of clarity. The relative abundances of all species experimentally detected are printed in bold. In addition, for all species with expected relative abundances > 1% that could not be detected experimentally, the absolute concentrations in mol/L are given in parentheses.

	1_1	1_2	2_1	2_2 10^{-7}	2_2 10^{-6}	2_2 10^{-5}	3_1	4_1	4_2
$(UO_2)_2CO_3(OH)_3^-$				7.3 ($4{\cdot}10^{-9}$)	**35.4**	**70.8**			
$Ca_2UO_2(CO_3)_3$	**10.1**	**46.6**	**71.2**	0.1					
$CaUO_2(CO_3)_3^{2-}$	**49.1**	**37.1**	**26.5**	0.1	0.1				
$MgUO_2(CO_3)_3^{2-}$	**10.3**	**10.8**	**1.8**	0.1	0.1		**9.0**		
$UO_2(CO_3)_2^{2-}$				2.2 ($2{\cdot}10^{-9}$)	1.6 ($2{\cdot}10^{-8}$)	0.7			
$UO_2(CO_3)_3^{4-}$	**30.5**	**5.4**	**0.4**	0.3	0.2	0.1	**90.7**		
$UO_2(OH)_2$				0.8	0.5	0.2			
UO_2^{2+}				**2.2**	**1.5**	**0.7**		14.0	12.0
UO_2CO_3				**77.2**	**53.7**	**24**			
UO_2HPO_4				1.2 ($1{\cdot}10^{-9}$)	0.8	0.4			
UO_2OH^+				**8.1**	**5.7**	**2.5**			
UO_2SO_4								69.4	62.6
$UO_2(SO_4)_2^{2-}$								13.8	24.1

evaluation of the fluorescence lifetimes gives comparable results for both samples. Due to the experimental difficulties described above, no clear statement can be made here.

5. Conclusions and outlook

It has been found that common thermodynamic databases for geochemical modelling software differ strongly in completeness, consistency and recent knowledge about uranium speciation in aquatic environments. This affects especially stable earth alkali uranyl carbonate and low dissolvable phosphate uranyl complexes that are highly relevant for migration behavior of uranium in neutral and alkaline systems. This paper not only strives to increase the sensitivity of geochemical modelers for this fundamental issue. Furthermore, it attempts to optimize the thermodynamic database and evaluate its validity for various natural high uranium aquatic systems.

The optimized database was evaluated using model calculations and comparative laboratory experiments applying time-resolved laser fluorescence spectroscopy (TRLFS), extraction experiments and orbitrap mass spectrometry. The results reflect the capabilities as well as limitations of these advanced analytical techniques to quantify uranyl speciation in natural water. In the case of model system 2_2, a concentration series with uranium concentrations of 10^{-5}, 10^{-6} und 10^{-7} mol/L was prepared and used for evaluation because the concentration of uranium in the natural analogue was below the detection limits of TRLFS and Orbitrap-MS. While some contradictions remain for the acidic waters, in the cases of all neutral and alkaline systems, at least the two, in most cases the three, species with the highest expected relative abundances could be confirmed.

The presented database is inherently consistent. Keeping the above mentioned analytical capabilities in mind, it can be considered to meet the observed uranyl speciation distribution in the used neutral and alkaline model systems and comparable waters, such as shallow groundwater and pore water, reasonably well. Additional investigations are required for waters with significantly different compositions, such as acidic, sulfate dominated waters.

Acknowledgement

Financial support for this research was provided by the Federal Institute for Geosciences and Natural Resources. We thank Wismut GmbH for providing natural analogues for groundwater and pore water chemistry from uranium mining legacy sites, which enabled this study to select appropriate synthetic water compositions. The authors would like to thank Vivien Schulte for providing us with Fig. 1 and editing Figs. 2 and 3.

Appendix A. Supplementary data

Supplementary data to this article can be found online at https://doi.org/10.1016/j.apgeochem.2018.10.006.

References

Agnes, G.R., Horlick, G., 1992. Electrospray mass-spectrometry as a technique for elemental analysis - preliminary results. Appl. Spectrosc. 46, 401–406.
Altmaier, M., Brendler, V., Bosbach, D., Kienzler, B., Marquardt, C., Neck, V., Richter, A., 2004. Sichtung. Zusammenstellung und Bewertung von Daten zur geochemischen Modellierung.
Altmaier, M., Brendler, V., Bube, C., Marquardt, C., Moog, H.C., Richter, A., Scharge, T., Voigt, W., Wilhelm, S., Wilms, T., Wollmann, G., 2011. THEREDA - Thermodynamische Referenzdatenbasis. GRS.
Altmaier, M., Fanghänel, T., Neck, V., 2006. Solubility of Uranium(VI) in Dilute to Concentrated NaCl, $MgCl_2$ and $CaCl_2$ Solutions.
Ball, J.W., Nordstrom, D.K., 1991. WATEQ4F Database. US Geological Survey.
Bernhard, G., Geipel, G., Brendler, V., Nitsche, H., 1996. Speciation of uranium in seepage waters of a mine tailing pile studied by time-resolved laser-induced fluorescence spectroscopy (TRLFS). Radiochim. Acta 74, 87–91.
Bernhard, G., Geipel, G., Brendler, V., Nitsche, H., 1998. Uranium speciation in waters of different uranium mining areas. J. Alloy. Comp. 271, 201–205.
Brönsted, J.N., 1922. Studies on solubility. IV. The principle of the specific interaction of ions. J. Am. Chem. Soc. 44, 877–898.
Brown, P.L., Ekberg, C., 2016. Hydrolysis of Metal Ions. Wiley.
Dong, W., Brooks, S.C., 2006. Determination of the formation constants of ternary complexes of uranyl and carbonate with alkaline earth metals (Mg^{2+}, Ca^{2+}, Sr^{2+}, and Ba^{2+}) using anion exchange method. Environ. Sci. Technol. 40, 4689–4695.
Dong, W., Brooks, S.C., 2008. Formation of aqueous $MgUO_2(CO_3)_3^{2-}$ complex and uranium anion exchange mechanism onto an exchange resin. Environ. Sci. Technol. 42, 1979–1983.
Finch, R., Murakami, T., 1999. Systematics and paragenesis of uranium minerals. Rev. Mineral. Geochem. 91–179.
Freyer, M., Walther, C., Stumpf, T., Buckau, G., Fanghänel, T., 2009. Formation of Cm Humate Complexes in aqueous solution at pH 3 to 5.5: the role of fast interchange. Radiochim. Acta 97, 547–558.
Galindo, C., Del Nero, M., 2013. Trace level uranyl complexation with phenylphosphonic acid in aqueous solution: direct speciation by high resolution mass spectrometry. Inorg. Chem. 52, 4372–4383.
Geipel, G., Amayri, S., Bernhard, G., 2008. Mixed complexes of alkaline earth uranyl carbonates: a laser-induced time-resolved fluorescence spectroscopic study. Spectrochim. Acta Mol. Biomol. Spectrosc. 71, 53–58.
Geipel, G., Brachmann, A., Brendler, V., Bernhard, G., Nitsche, H., 1996. Uranium(VI) sulfate complexation studied by time-resolved laser-induced fluorescence spectroscopy (TRLFS). Radiochim. Acta 75 (4), 199–204.
Gorman-Lewis, D., Fein, J.B., Burns, P.C., Szymanowski, J.E.S., Converse, J., 2008. Solubility measurements of the uranyl oxide hydrate phases metaschoepite, compreignacite, Na–compreignacite, becquerelite, and clarkeite. J. Chem. Therm. 40, 980–990.
Gorman-Lewis, D., Mazeina, L., Fein, J.B., Szymanowski, J.E.S., Burns, P.C., Navrotsky, A., 2007. Thermodynamic properties of soddyite from solubility and calorimetry measurements. J. Chem. Thermodyn. 39, 568–575.
Gorman-Lewis, D., Shvareva, T., Kubatko, K.A., Burns, P.C., Wellman, D.M., McNamara, B., Szymanowski, J.E.S., Navrotsky, A., Fein, J.B., 2009. Thermodynamic properties of autunite, uranyl hydrogen phosphate, and uranyl orthophosphate from solubility and calorimetric measurements. Environ. Sci. Technol. 43, 7416–7422.

Grenthe, I., Fuger, J., Konings, R.J.M., Lemire, R.J., Muller, A.B., Nguyen-Trung, C., Wanner, H., 1992. Chemical Thermodynamics of Uranium.
Grive, M., Duro, L., Colas, E., Giffaut, E., 2015. Thermodynamic data selection applied to radionuclides and chemotoxic elements: an overview of the ThermoChimie-TDB. Appl. Geochem. 55, 85–94.
Guillaumont, R., Fanghänel, T., Fuger, J., Grenthe, I., Neck, V., Palmer, D.A., Rand, M.H., 2003. Update on the Chemical Thermodynamics of U, Am, Np, Pu and Tc. Elsevir, Amsterdam.
Hakam, O.K., Choukri, A., Moutia, Z., Chouak, A., Cherkaoui, R., Reyss, J.L., Lferde, M., 2001a. Uranium and radium in groundwater and surface water samples in Morocco. Radiat. Phys. Chem. 61, 653–654.
Hakam, O.K., Choukri, A., Reyss, J.L., Lferde, M., 2000. Activities and activity ratios of U and Ra radioisotopes in drinking wells, springs and tap water samples in Morocco. Radiochim. Acta 88, 55–60.
Hakam, O.K., Choukri, A., Reyss, J.L., Lferde, M., 2001b. Determination and comparison of uranium and radium isotopes activities and activity ratios in samples from some natural water sources in Morocco. J. Environ. Radioact. 57, 175–189.
Hummel, W., Anderegg, G., Puigdomènech, I., Rao, L., Tochiyama, O., 2005. PSI/Nagra Chemical Thermodynamic Database 12/07. PSI/Nagra, Amsterdam.
Kimura, T., Choppin, G.R., 1994. Luminescence study on determination of the hydration number of Cm(III). J. Alloy. Comp. 213, 313–317.
Langmuir, D., 1997. Aqueous Environmental Geochemistry. Prentice Hall.
Mahoney, J.J., 2013. Sensitivity of database selection in modeling the transport of uranium. In: Annual International Mine Water Association Conference – Reliable Mine Water Technology (IMWA 2013), Golden, Colorado, USA.
Meinrath, G., Volke, P., Helling, C., Dudel, E.G., Merkel, B.J., 1999. Determination and interpretation of environmental water samples contaminated by uranium mining activities. Fresen. J. Anal. Chem. 364, 191–202.
Moog, H.C., Bok, F., Marquardt, C.M., Brendler, V., 2015. Disposal of nuclear waste in host rock formations featuring high-saline solutions – implementation of a thermodynamic reference database (THEREDA). Appl. Geochem. 55, 72–84.
Moulin, C., Charron, N., Plancque, G., Virelizier, H., 2000. Speciation of uranium by electrospray ionization mass spectrometry: comparison with time-resolved laser-induced fluorescence. Appl. Spectrosc. 54, 843–848.
Muto, T., Hirono, S., Kurata, H., 1965. Some aspects of fixation of uranium from natural waters. Min. Geol. 15, 287–298.
Muto, T., Hirono, S., Kurata, H., 1968. Some Aspects of Fixation of Uranium from Natural Waters. Japan Atomic Energy Research Inst.
Neck, V., Fanghänel, T., Metz, V., Kienzler, B., 2001. Kenntnisstand zur aquatischen Chemie und der thermodynamischen Datenbasis von Actiniden und Technetium. In: Abschlussbericht zum BfS-Projekt „Erstellung eines Nahfeldmodells von Gebinden hochradioaktiver Abfälle im Salzstock Gorleben: geochemisch fundierter Quellterm für HAW-Glas, abgebrannte Brennelemente und Zement. Forschungszentrum Karlsruhe.
Osman, A.A.A., Geipel, G., Bernhard, G., Worch, E., 2013. Investigation of uranium binding forms in selected German mineral waters. Environ. Sci. Pollut. Control Ser. 20 (12), 8629–8635.
Parkhurst, D.L., Appelo, C.A.J., 1999. User's Guide to PHREEQC (Version 2): a Computer Program for Speciation, Batch-reaction, One-dimensional Transport, and Inverse Geochemical Calculations, Water-resources Investigations Report. - ed. .
Post, V.E.A., Vassolo, S.I., Tiberghien, C., Baranyikwa, D., Miburo, D., 2017. Weathering and evaporation controls on dissolved uranium concentrations in groundwater – a case study from northern Burundi. Sci. Total Environ. 607–608, 281–293.
Rai, D., Felmy Andrew, R., Hess Nancy, J., Moore Dean, A., Yui, M., 1998. A thermodynamic model for the solubility of UO2(am) in the aqueous K^+-Na^+-HCO_3^--CO_3^{2-}-OH^--H_2O system. Radiochim. Acta 17.
Richter, A., Bok, F., Brendler, V., 2015. Data compilation and evaluation of U(IV) and U (VI) for the thermodynamic reference database THEREDA. https://www.thereda.de/de/.
Sandino, M.C.A., Grambow, B., 1994. Solubility equilibria in the U(VI)-Ca-K-Cl-H_2O system: transformation of schoepite into bequerelite and compreignacite. Radiochim. Acta 66–7, 37–43.
Schreyer, J.M., Baes, C.F., 1954. The solubility of uranium(VI) orthophosphates in phosphoric acid solutions. J. Am. Chem. Soc. 76, 354–357.
Silva, R.J., Nitsche, H., 1995. Actinide environmental chemistry. Radiochim. Acta 377.
Skeppström, K., Olofsson, B., 2007. Uranium and radon in groundwater - an overview of the problem. European Water 17/18, 51–62.
Smith, B., Hutchins, M.G., Powell, J.H., Talbot, D., Trick, J.K., Gedeon, R., Amro, H., Kilani, S., Constantinou, G., Afrodisis, S., Constantinou, C., 2000. The Distribution of Natural Radioelements in Ground Waters and Post-Cretaceous Sediments from the Southern Mediterranean Margin.
Steudtner, R., Arnold, T., Geipel, G., Bernhard, G., 2010. Fluorescence spectroscopic study on complexation of uranium(VI) by glucose: a comparison of room and low temperature measurements. J. Radioanal. Nucl. Chem. 284 (2), 421–429.
Vercouter, T., Reiller, P.E., Ansoborlo, E., Février, L., Gilbin, R., Lomenech, C., Philippini, V., 2015. A modelling exercise on the importance of ternary alkaline earth carbonate species of uranium(VI) in the inorganic speciation of natural waters. Appl. Geochem. 55, 192–198.
Vercouter, T., Vitorge, P., Amekraz, B., Moulin, C., 2008. Stoichiometries and thermodynamic stabilities for aqueous sulfate complexes of U(VI). Inorg. Chem. 47, 2180–2189.
Wang, Z., Zachara John, M., Liu, C., Gassman, P.L., Felmy Andrew, R., Clark Sue, B., 2008. A cryogenic fluorescence spectroscopic study of uranyl carbonate, phosphate and oxyhydroxide minerals. Radiochim. Acta Int. J. Chem. Aspects Nuclear Sci. Technol. 591.
Wang, Z.M., Zachara, J.M., Yantasee, W., Gassman, P.L., Liu, C.X., Joly, A.G., 2004. Cryogenic laser induced fluorescence characterization of U(VI) in hanford vadose zone pore waters. Environ. Sci. Technol. 38, 5591–5597.